



1 **Mass Accommodation and Gas-Particle Partitioning in Secondary**  
2 **Organic Aerosols: Dependence on Diffusivity, Volatility, Particle-**  
3 **phase Reactions, and Penetration Depth**

4

5 Manabu Shiraiwa<sup>1,\*</sup> and Ulrich Pöschl<sup>2,\*</sup>

6

7 1. Department of Chemistry, University of California, Irvine, CA92625, USA

8 2. Multiphase Chemistry Department, Max Planck Institute for Chemistry, 55128 Mainz, Germany

9 \* Correspondence to: [m.shiraiwa@uci.edu](mailto:m.shiraiwa@uci.edu); [u.poschl@mpic.de](mailto:u.poschl@mpic.de)

10



11 **Abstract.**

12 Mass accommodation is an essential process for gas-particle partitioning of organic compounds in  
13 secondary organic aerosols (SOA). The mass accommodation coefficient is commonly described  
14 as the probability of a gas molecule colliding with the surface to enter the particle phase. It is often  
15 applied, however, without specifying if and how deep a molecule has to penetrate beneath the  
16 surface to be regarded as incorporated into the condensed phase (adsorption vs. absorption). While  
17 this aspect is usually not critical for liquid particles with rapid surface-bulk exchange, it can be  
18 important for viscous semisolid or glassy solid particles to distinguish and resolve the kinetics of  
19 accommodation at the surface, transfer across the gas-particle interface, and further transport into  
20 the particle bulk.

21 For this purpose, we introduce a novel parameter: an effective mass accommodation coefficient  
22  $\alpha_{\text{eff}}$  that depends on penetration depth and is a function of surface accommodation coefficient,  
23 volatility, bulk diffusivity, and particle-phase reaction rate coefficient. Application of  $\alpha_{\text{eff}}$  in the  
24 traditional Fuchs-Sutugin approximation of mass-transport kinetics at the gas-particle interface  
25 yields SOA partitioning results that are consistent with a detailed kinetic multilayer model (KM-  
26 GAP, Shiraiwa et al. 2012) and two-film model solutions (MOSAIC, Zaveri et al., 2014) but  
27 deviate substantially from earlier modeling approaches not considering the influence of penetration  
28 depth and related parameters.

29 For highly viscous or semisolid particles, we show that the effective mass accommodation  
30 coefficient remains similar to the surface accommodation coefficient in case of low-volatile  
31 compounds, whereas it can decrease by several orders of magnitude in case of semi-volatile  
32 compounds. Such effects can explain apparent inconsistencies between earlier studies deriving  
33 mass accommodation coefficients from experimental data or from molecular dynamics  
34 simulations.

35 Our findings challenge the approach of traditional SOA models using the Fuchs-Sutugin  
36 approximation of mass transfer kinetics with a fixed mass accommodation coefficient regardless  
37 of particle phase state and penetration depth. The effective mass accommodation coefficient  
38 introduced in this study provides an efficient new way of accounting for the influence of volatility,  
39 diffusivity, and particle-phase reactions on SOA partitioning in process models as well as in  
40 regional and global air quality models.

41



## 42 **Introduction.**

43 Secondary organic aerosols (SOA) are major constituents of atmospheric particulate  
44 matter, affecting air quality, climate, and public health (Jimenez et al., 2009; Kanakidou et al.,  
45 2005; Pöschl and Shiraiwa, 2015; Shrivastava et al., 2017a). Gas-phase reactions of volatile  
46 organic compounds (VOC) emitted from various anthropogenic and biogenic sources with  
47 oxidants such as ozone and OH radicals lead to the formation and growth of SOA (Kroll and  
48 Seinfeld, 2008). The oxidation of VOC forms a myriad of semi-volatile (SVOC) and low volatility  
49 organic compounds (LVOC) that can condense on pre-existing particles (Ziemann and Atkinson,  
50 2012) or contribute to nucleation and new particle formation (Tröstl et al., 2016). The evolution of  
51 SOA is a complex multi-step process that involves chemical reactions and mass transport in the gas  
52 phase, at the particle surface and in the particle bulk, but the interplay of these processes and the  
53 rate-limiting steps in SOA formation have not yet been fully resolved/elucidated (Shiraiwa et al.,  
54 2014).

55 Traditionally, SOA particles were assumed to be homogeneous and well-mixed quasi-  
56 liquid droplets (Pankow, 1994). As demonstrated by recent atmospheric measurements and  
57 laboratory experiments, they can adopt glassy solid or amorphous semi-solid phase states,  
58 challenging the traditional views of SOA properties, interactions and effects (Koop et al., 2011;  
59 Reid et al., 2018; Virtanen et al., 2010). Slow diffusion of water, oxidants and organic molecules  
60 in viscous, semi-solid, or glassy particles may lead to kinetic limitations in heterogeneous and  
61 multiphase reactions (Alpert et al., 2019; Davies and Wilson, 2015; Kuwata and Martin, 2012;  
62 Shiraiwa et al., 2011; Zhang et al., 2018; Zhou et al., 2019). Global model calculations suggest  
63 that the phase state of atmospheric SOA may vary between liquid, semi-solid and solid in the  
64 planetary boundary layer, while SOA should be mostly in a glassy state in the free troposphere  
65 (Shiraiwa et al., 2017). The occurrence of glassy SOA in the free troposphere may promote ice  
66 nucleation and cloud droplet activation (Knopf et al., 2018; Slade et al., 2017) and facilitate long-  
67 range transport of toxic organic compounds contained in SOA (Mu et al., 2018; Shrivastava et al.,  
68 2017b).

69 The formation and properties of SOA are large sources of uncertainty in the current  
70 understanding of global air quality, climate change, and public health. The development of SOA  
71 models is among the most challenging problems in atmospheric chemistry (Tsigaridis et al., 2014).  
72 In most current air quality, atmospheric chemistry and climate models, the limiting step of SOA



73 formation is assumed to be gas-phase oxidation of VOC to form semi-volatile and low volatile  
74 products. Thus, gas-phase oxidation is described kinetically, while gas-particle partitioning is often  
75 approximated by quasi-instantaneous equilibrium partitioning of the oxidation products (Pankow,  
76 1994; Shrivastava et al., 2017a; Tsigaridis et al., 2014). The assumption of quasi-instantaneous  
77 gas-particle equilibration, however, is in question if particles are highly viscous, semi-solid or  
78 glassy - especially at low temperatures and low relative humidity (RH) (Li and Shiraiwa, 2019;  
79 Shiraiwa and Seinfeld, 2012). Experimental studies found kinetic limitations for gas uptake and  
80 particle evaporation at low RH (Liu et al., 2016; Perraud et al., 2012; Vaden et al., 2011; Yli-Juuti  
81 et al., 2017), but not for mixing in SOA at medium or high RH (Ye et al., 2016; Ye et al., 2018).  
82 An appropriate treatment of kinetic limitations depending on ambient conditions is critical for  
83 accurately reproducing particle size distribution dynamics in SOA growth (Shiraiwa et al., 2013a;  
84 Zaveri et al., 2018; Zaveri et al., 2020).

85 The dynamics of gas-particle partitioning have been considered in a wide range of  
86 atmospheric aerosol models, including aerosol dynamics models (Liu et al., 2019; McVay et al.,  
87 2014; Pandis et al., 1993; Riipinen et al., 2011; Zaveri et al., 2014), kinetic multilayer models  
88 (Berkemeier et al., 2016; Fowler et al., 2018; Roldin et al., 2014; Shiraiwa et al., 2012), GECKO-  
89 A (Aumont et al., 2005), the volatility basis set approach (Trump and Donahue, 2014; Trump et  
90 al., 2014), the statistical oxidation model (Cappa et al., 2016; Jathar et al., 2016), and particle  
91 evaporation models (Vaden et al., 2011; Yli-Juuti et al., 2017). Most model studies are using the  
92 Fuchs-Sutugin approximation of mass-transport kinetics at the gas-particle interface with a fixed  
93 mass accommodation coefficient that does not vary with particle phase state nor with the volatility  
94 and diffusivity of the investigated organic compounds. Molecular dynamics simulations (Julin et  
95 al., 2014; Von Domaros et al., 2020) and a recent SOA chamber study (Liu et al., 2019) suggest  
96 that the mass accommodation coefficients for semi-volatile organic molecules on organic  
97 substrates are close to unity. Measurement-derived mass accommodation coefficients reported  
98 from thermodenuder investigations of SOA volatility distributions, however, were one to three  
99 orders of magnitude lower (Kostenidou et al., 2018; Lee et al., 2010; Saleh et al., 2011).

100 Overall, the relations between particle phase state, mass accommodation, and the growth  
101 and atmospheric evolution of SOA have not yet been resolved and continue to be a subject of  
102 scientific debate. In this study, we investigate the influence of volatility, diffusivity, and particle  
103 phase state on the mass accommodation and gas-particle partitioning of organic compounds in



104 SOA by detailed and simplified kinetic modeling approaches, comparing the Fuchs-Sutugin  
105 approximation to a detailed kinetic multilayer model (KM-GAP, Shiraiwa et al. 2012) as well as  
106 approximate and transient two-film model solutions (MOSAIC, Zaveri et al., 2014).

107

## 108 Theory and Methods

109 Traditionally, dynamic models of aerosol chemistry and physics describe the rate of gas-  
110 particle partitioning by a first-order gas-particle mass transfer coefficient ( $k_{gp}$  in  $s^{-1}$ ) based on the  
111 Fuchs-Sutugin approximation of gas diffusion in the transition regime (Seinfeld and Pandis, 2016):

$$112 \quad k_{gp} = 4 \pi D_g r_p N_p \beta \quad (1)$$

$$113 \quad \beta = \frac{0.75 \alpha (1+Kn)}{Kn^2 + Kn + 0.283 Kn \alpha + 0.75 \alpha} \quad (2)$$

114 where  $D_g$  ( $cm^2 s^{-1}$ ) is the gas phase diffusivity,  $r_p$  (cm) is the particle radius,  $N_p$  ( $cm^{-3}$ ) is the particle  
115 number concentration,  $Kn$  is the Knudsen number, and  $\alpha$  is the mass accommodation coefficient  
116 which represents the probability for a gas molecule colliding with the surface of the particles to  
117 enter the condensed phase.  $Kn$  is the ratio of the mean free path in the gas phase ( $\lambda$ ), which can be  
118 calculated using the mean thermal velocity ( $\omega$ ), and the particle radius:  $Kn = \lambda / r_p = 3 D_g / (\omega r_p)$   
119 (Pöschl et al., 2007). Note that  $k_{gp}$  is also often termed as condensation sink (CS). According to  
120 the absorptive partitioning theory under the assumption of ideal mixing (Pankow, 1994; Trump  
121 and Donahue, 2014), the rate of change of the gas- and particle-phase mass concentrations ( $C^g$ ,  $C^p$ )  
122 of an organic compound in SOA partitioning can be expressed as:

$$123 \quad \frac{dC^g}{dt} = -k_{gp} \left( C^g - \frac{C^g}{C_{OA}} C^0 \right) \quad (3)$$

$$124 \quad \frac{dC^p}{dt} = k_{gp} \left( C^g - \frac{C^p}{C_{OA}} C^0 \right) - k_b C^p \quad (4)$$

125 where  $C_{OA}$  ( $\mu g m^{-3}$ ) is the organic aerosol particle mass concentration,  $C^0$  ( $\mu g m^{-3}$ ) is the gas phase  
126 saturation mass concentration of the pure organic compound, and  $k_b$  ( $s^{-1}$ ) is the first-order rate  
127 coefficient for its reaction in the particle bulk. The term  $\frac{C^p}{C_{OA}} C^0$  represents gas-phase concentration  
128 of Z right at the surface and condensation is driven by gas-phase concentration gradient of Z  
129 between the gas and condensed phases.

130 While the term mass accommodation coefficient is widely used in atmospheric aerosol  
131 studies, its precise meaning is not always well defined. In particular,  $\alpha$  is often applied without  
132 specifying if and how deep a molecule has to penetrate beneath the surface to have entered the



133 condensed phase (adsorption vs. absorption). This aspect is usually not critical for liquid droplets  
134 with rapid surface-bulk exchange, fast bulk diffusion, and swift equilibration between the  
135 condensed phase and the surrounding gas phase. For viscous or solid particles, however, it can be  
136 essential to distinguish and resolve the kinetics of surface and bulk processes, including  
137 accommodation at the surface, transfer across the gas-particle interface, and further transport into  
138 the particle bulk (Kolb et al., 2010; Pöschl et al., 2007; Shiraiwa et al., 2012).

139 Building on the PRA kinetic model framework (Pöschl et al., 2007) and the kinetic  
140 multilayer model of surface chemistry and gas-particle interactions in aerosols and clouds (KM-  
141 GAP; Shiraiwa et al., 2012), we have derived an expression for the mass accommodation  
142 coefficient as a function of penetration depth into the particle bulk and related parameters (see  
143 step-by-step derivation in Appendix):

$$144 \quad \alpha(x) = \alpha_s \frac{1}{1 + \frac{\alpha_s \omega C^0}{4 D_b \rho_p} x \cdot 10^{-12} \frac{\text{g cm}^{-3}}{\mu\text{g m}^{-3}}} \quad (5)$$

145 Here  $\omega$  ( $\text{cm s}^{-1}$ ) is the mean thermal velocity of the organic compound in the gas phase,  $D_b$  ( $\text{cm}^2$   
146  $\text{s}^{-1}$ ) is its diffusivity in the condensed phase,  $\rho_p$  ( $\text{g cm}^{-3}$ ) is the particle density, and  $x$  ( $\text{cm}$ ) is the  
147 penetration depth. The scaling factor  $10^{-12} (\text{g cm}^{-3})/(\mu\text{g m}^{-3})$  allows for inserting  $C^0$  in the  
148 commonly used units of  $\mu\text{g m}^{-3}$ ; it can be omitted when  $C^0$  is inserted in  $\text{g cm}^{-3}$  or when all  
149 quantities are inserted with standard SI units (cgs or mks system of units).

150 The surface accommodation coefficient  $\alpha_s$ , which corresponds to  $\alpha(0)$  with the penetration  
151 depth of 0, is the probability for a gas molecule  $Z$  colliding with the surface not to be immediately  
152 scattered back to the gas phase but to be accommodated at the surface for period longer than the  
153 duration of an elastic scattering process (Pöschl et al., 2007). Various equivalent, similar or closely  
154 related terms and parameters have been defined and used in the scientific literature include (Kolb  
155 et al., 2010; Pöschl et al., 2007): the condensation coefficient (Pruppacher and Klett, 1997),  
156 adsorption coefficient (Shi et al., 1999; Turco et al., 1989; Worsnop et al., 2002), sticking  
157 coefficient (Hanson, 1997), sticking probability (Clement et al., 1996; Garrett et al., 2006),  
158 trapping probability (Masel, 1996), adsorptive mass accommodation coefficient (Elliott et al.,  
159 1991), and thermal accommodation coefficient (Li et al., 2001; Worsnop et al., 2002).

160 When the penetration depth equals one or two molecular layers, i.e., once or twice the  
161 effective molecular length or diameter ( $\delta$ ), the corresponding penetration-depth-dependent mass



162 accommodation coefficient is equivalent to the quasi-static surface accommodation coefficient  
163 ( $\alpha_{ss}$ ) or bulk accommodation coefficient ( $\alpha_b$ ), respectively, as defined in earlier kinetic multilayer  
164 model studies (Shiraiwa et al., 2012):  $\alpha(\delta) = \alpha_{ss}$  and  $\alpha(2\delta) = \alpha_b$ . A recent study has compared this  
165 kinetic multilayer (KM) modeling approach with molecular dynamics (MD) simulations to  
166 calculate mass accommodation coefficients for a variety of semi-volatile compounds with different  
167 volatilities in squalene (Von Domaros et al., 2020). The penetration depth was assumed to be equal  
168 to the sum of half of the molecule's own length and half of the length of a squalene molecule. For  
169 the evaluation of uncertainties and sensitivities, the penetration depth was also varied from semi-  
170 volatile molecule's own length as a lower bound to the half-width of the nonuniform free energy  
171 region determined by the MD free energy profile as an upper bound. Within this range, the results  
172 of MD and KM simulations were in good agreement with each other, confirming the consistency  
173 and validity of the multilayer approach (Von Domaros et al., 2020).

174 Using the two-film theory of mass transfer between gas and particle phase, Zaveri et al.  
175 (2014) showed that the effects of a concentration gradient in the particle can be represented by a  
176 thin film adjacent to the surface with the following thickness or effective penetration depth for  
177 non-reactive partitioning and reactive uptake, respectively:

$$178 \quad x_{\text{eff}} = r_p / 5 \quad (\text{non-reactive partitioning}) \quad (6)$$

$$179 \quad x_{\text{eff}} = r_p \left( \frac{1-Q}{q \coth q - 1} \right) \quad (\text{reactive uptake}) \quad (7)$$

180 where  $Q$  is the ratio of the average particle-phase concentration to the surface concentration at  
181 steady state and  $q$  is a dimensionless diffusion-reaction parameter (Seinfeld and Pandis, 2016):

$$182 \quad Q = 3 \left( \frac{q \coth q - 1}{q^2} \right) \quad (8)$$

$$183 \quad q = r_p \sqrt{\frac{k_b}{D_b}} \quad (9)$$

184 Note that  $q_Z$  is the ratio of the particle radius to the so-called reacto-diffusive length,  $(D_b/k_b)^{0.5}$ ,  
185 representing the characteristic depth to which a species can penetrate while reacting in the particle  
186 bulk (Pöschl et al., 2007; Worsnop et al., 2002).

187 By inserting  $x_{\text{eff}}$  in equation (5), we obtain an effective mass accommodation coefficient  
188 that accounts for the influence of penetration depth and its dependence on the diffusivity and  
189 reactivity of the investigated chemical species in the particle:



190 
$$\alpha_{\text{eff}} = \alpha(x_{\text{eff}}) \quad (10)$$

191

## 192 **Results and Discussion**

193 To investigate and demonstrate the relevance of the kinetics of mass accommodation and  
194 the applicability of  $\alpha_{\text{eff}}$ , we simulate the temporal evolution of partitioning and equilibration of  
195 semi-volatile organic compounds (SVOC) with  $C^0 = 100 \mu\text{g m}^{-3}$  and  $D_g = 0.1 \text{ cm}^2 \text{ s}^{-1}$  interacting  
196 with non-volatile seed particles with a number concentration of  $5000 \text{ cm}^{-3}$ , an initial diameter of  
197 200 nm, and a surface accommodation coefficient  $\alpha_s = \alpha(0) = 1$ . For the SVOC, we assume initial  
198 gas- and particle-phase concentrations of  $2 \mu\text{g m}^{-3}$  and  $0 \mu\text{g m}^{-3}$ , respectively. The particles are  
199 assumed to be either liquid with a bulk diffusion coefficient  $D_b = 10^{-7} \text{ cm}^2 \text{ s}^{-1}$  or semisolid with  $D_b$   
200  $= 10^{-15} \text{ cm}^2 \text{ s}^{-1}$ .

201 Model calculations were performed with the detailed kinetic multilayer model of gas-  
202 particle interactions (KM-GAP, Shiraiwa et al. 2012), with the Model for Simulating Aerosol  
203 Interactions and Chemistry (MOSAIC; Zaveri et al., 2014), and with an aerosol dynamic model  
204 using the simple Fuchs-Sutugin gas-phase diffusion model (F-S) with different values of  $\alpha_m$ . Here,  
205 the KM-GAP results can be regarded as a benchmark, because the KM-GAP model explicitly  
206 resolves all relevant processes - including gas diffusion, reversible adsorption, surface-bulk  
207 exchange, bulk diffusion, and condensed-phase reactions - and has been successfully validated by  
208 against experimental data of both non-reactive partitioning and reactive gas uptake in a wide range  
209 of aerosol and surrogate systems (Berkemeier et al., 2017; Shiraiwa et al., 2012). The MOSAIC  
210 model yields approximate and transient solutions building on a less detailed representation of gas-  
211 particle interactions, which does not resolve reversible adsorption and surface-bulk exchange  
212 (Zaveri et al., 2014). In the F-S approximation, the kinetics of particle-phase mass transport are  
213 represented only by  $\alpha_m$  as inserted into Eq. (2).

214 For liquid particles with fast surface-bulk exchange and bulk diffusion ( $D_b = 10^{-7} \text{ cm}^2 \text{ s}^{-1}$ ),  
215  $\alpha(x)$  remains close to  $\alpha_s = \alpha(0) = 1$ , and all models yield the same result of fast mass transfer from  
216 the gas to particle phase and equilibration within one second. For semi-solid particles with  $D_b =$   
217  $10^{-15} \text{ cm}^2 \text{ s}^{-1}$ , however, the temporal evolution of the SVOC gas-phase and particle-phase  
218 concentrations varies between different models and different values of  $\alpha$  as shown in Figure 1 on  
219 logarithmic scales.





220 According to KM-GAP (black line), the initial uptake of SVOC by the semisolid particle  
221 phase is as fast as approximated by F-S with  $\alpha = \alpha_{ss} = \alpha_z(\delta) = 3 \times 10^{-2}$  corresponding to a  
222 penetration depth of only one molecular length (monolayer) below the particle surface. After one  
223 second, however, the KM-GAP uptake is limited by bulk diffusion and slows down substantially.  
224 After about one hour, KM-GAP converges with the F-S approximation using  $\alpha = \alpha_{\text{eff}} = \alpha(r_p/5) =$   
225  $8 \times 10^{-4}$ . Notably, the F-S approximation with  $\alpha_{\text{eff}}$  is identical to the MOSAIC approximation,  
226 although the latter is based on different rate equations using a unity mass accommodation  
227 coefficient like KM-GAP ( $\alpha_s = 1$ ) and a two-film approach of bulk diffusion (Zaveri et al., 2014).  
228 The MOSAIC transient solution exhibits a very high and likely overestimated initial uptake  
229 corresponding to the F-S approximation with  $\alpha = \alpha_s = 1$ , because it does not resolve reversible  
230 adsorption and desorption at the surface (Shiraiwa et al., 2012). After  $\sim 1$  min, however, the  
231 MOSAIC transient solution converges with KM-GAP. Overall, Figure 1 demonstrates that  
232 accurate modeling of SVOC partitioning and uptake into semisolid particles requires an explicit  
233 treatment of reversible adsorption and desorption at short time scales ( $< 1$  min) and an explicit  
234 treatment of bulk diffusion at intermediate time scales ( $\sim 1$  min to  $\sim 1$  h). At long timescales ( $> 1$   
235 h), the partitioning is reasonable well captured by both the MOSAIC approximation using a two-  
236 film approach of bulk diffusion (Zaveri et al., 2014) as well as the simple F-S approximation  
237 accounting for the influence of penetration depth with the effective mass accommodation  
238 coefficient,  $\alpha_{\text{eff}}$ , newly introduced this study.

239 Figure 2a shows the temporal evolution of the gas-phase concentration of organic  
240 compounds with different volatilities ( $C^0 = 0.1$  to  $1000 \mu\text{g m}^{-3}$ ) that undergo non-reactive  
241 partitioning into semisolid seed aerosol particles ( $D_b = 10^{-15} \text{ cm}^2 \text{ s}^{-1}$ ). At short timescales,  
242 substantial deviations can occur for semi-volatile compounds ( $C^0 = 1$  to  $100 \mu\text{g m}^{-3}$ ), but at longer  
243 time scales KM-GAP and the F-S approximation with  $\alpha_{\text{eff}}$  are in reasonably good agreement  
244 (relative deviations  $< 10\%$  after  $\sim 1$  h). For low-volatile compounds ( $C^0 < 1 \mu\text{g m}^{-3}$ ), equilibration  
245 is achieved faster than for semi-volatile compounds because local thermodynamic equilibrium  
246 between the gas phase and the particle surface is quickly established by condensation without  
247 significant re-evaporation (Li and Shiraiwa, 2019; Zaveri et al., 2014). Semi-volatile compounds  
248 with reactive functional groups can undergo particle-phase reactions such as dimerization and  
249 oligomerization (Ziemann and Atkinson, 2012). Peroxide-containing highly oxidized molecules



250 (HOM) are labile with chemical half-lives shorter than one hour (Krapf et al., 2016; Tong et al.,  
251 2016; Tong et al., 2019), and a recent study has shown that particle-phase reactions must be  
252 considered to describe HOM effects on particle growth (Pospisilova et al., 2020). Model results  
253 for SVOC partitioning plus reactive uptake with different rate coefficients in semisolid aerosol  
254 particles are shown in Figure 2b. The results of the Fuchs-Sutugin approximation with  $\alpha_{\text{eff}} = \alpha(x_{\text{eff}})$   
255 and  $x_{\text{eff}}$  from Eq. 7 are identical to the MOSAIC approximate and transient solutions. The uptake  
256 predicted by KM-GAP is similar but slightly slower in case of high bulk reaction rate coefficients,  
257 which can be attributed to the influence of reversible adsorption and desorption at the surface.  
258 Additional simulations with  $\alpha_s = 0.1$  confirm that the results of the Fuchs-Sutugin approximation  
259 with  $\alpha_{\text{eff}}$  and the MOSAIC approximate solution are identical, and that the results of KM-GAP and  
260 the MOSAIC transient solution are similar (Fig. S1).

261 For a given surface accommodation coefficient of  $\alpha_s = 1$ , which is likely a good  
262 approximation for SVOC on organic surfaces (Julin et al., 2014; Von Domaros et al., 2020),  
263 Figures 3a and 3b show how the effective mass accommodation coefficient  $\alpha_{\text{eff}}$  depends on  
264 volatility and bulk diffusivity as related to particle phase state and viscosity according to the  
265 Stokes-Einstein relation (Shiraiwa et al., 2011). In the liquid phase with high bulk diffusivity ( $D_b$   
266  $> 10^{-10} \text{ cm}^2 \text{ s}^{-1}$ ),  $\alpha_{\text{eff}}$  is essentially the same as  $\alpha_s$  independent of volatility ( $\alpha_{\text{eff}} \approx \alpha_s \approx 1$ ). With a  
267 decrease of bulk diffusivity in viscous or semisolid particles,  $\alpha_{\text{eff}}$  decreases substantially for SVOC  
268 ( $0.3 < C^0 < 300 \mu\text{g m}^{-3}$ ) and so-called intermediate volatility organic compounds (IVOC;  $300 < C^0$   
269  $< 3 \times 10^6 \mu\text{g m}^{-3}$ ) but not for LVOC ( $3 \times 10^{-4} < C^0 < 0.3 \mu\text{g m}^{-3}$ ) and so-called extremely low-volatile  
270 organic compounds (ELVOC;  $C^0 < 3 \times 10^{-4} \mu\text{g m}^{-3}$ ). The reason why compounds with higher  
271 volatility are more strongly affected by particle phase state and diffusivity is that they are more  
272 likely to desorb back to the gas phase when diffusion into the bulk is slow. Compounds with lower  
273 volatility exhibit much lower desorption rates and are less likely to re-evaporate even if their  
274 diffusion into the bulk is slow. On the other hand, the influence of particle phase state and  
275 diffusivity increases with particle size because longer pathways of diffusion are required for  
276 effective accommodation, penetration, and absorption of gas molecules into larger particles as  
277 illustrated in Figures 3c and 3d.

278 The theoretically predicted influence of volatility on effective mass accommodation is  
279 consistent with a recent experimental study of  $\alpha$ -pinene SOA reporting that the observed mass  
280 accommodation coefficients decreased from  $\sim 1$  for low-volatile compounds to  $\sim 0.3$  for semi-



281 volatile compounds (Liu et al., 2019). Particle viscosity and bulk diffusivity were not reported for  
282 these experiments, but values around  $10^{-13}$  to  $10^{-14}$   $\text{cm}^2 \text{s}^{-1}$  had previously been estimated for the  
283 diffusion coefficient of organic compounds in  $\alpha$ -pinene SOA under dry conditions (Zhou et al.,  
284 2013). As illustrated in Figure 4a, theoretical predictions of  $\alpha_{\text{eff}}$  assuming  $\alpha_s = 1$  and  $D_b = 10^{-12}$  to  
285  $10^{-14}$   $\text{cm}^2 \text{s}^{-1}$  approximately capture the decrease and encompass the variability and uncertainty  
286 range of the experimentally derived mass accommodation coefficients reported by (Liu et al.,  
287 2019). Indeed, the observational  $\alpha_m$  values reported in (Liu et al., 2019) and other experimental  
288 studies are usually obtained by fitting measurement data with the F-S approximation, and thus they  
289 should be directly compared to effective mass accommodation coefficient  $\alpha_{\text{eff}}$  as derived by  
290 integration of the F-S approximation with detailed kinetic models of mass transport across the gas-  
291 particle interface. Figure 4b shows a wide range of other measurement-derived mass  
292 accommodation coefficients for various SOA and surrogate systems (data points/shaded areas) in  
293 comparison to generic values of  $\alpha_{\text{eff}}$  (lines) calculated for characteristic experimental conditions  
294 ( $\omega = 2.0 \times 10^4$   $\text{cm s}^{-1}$ ,  $\rho_p = 1$   $\text{g cm}^{-3}$ , and  $r_p = 100$   $\text{nm}$ , and  $D_b = 10^{-19}$  to  $10^{-5}$   $\text{cm}^2 \text{s}^{-1}$ ). As indicated  
295 by molecular dynamics simulations and related studies, the surface accommodation coefficient  
296 (adsorption probability) for semi-volatile or low-volatile organic compounds on organic surfaces  
297 is likely close to unity,  $\alpha_s = 1$  (Julin et al., 2014; Von Domaros et al., 2020). Accordingly, low  
298 observational values of  $\alpha$  can be attributed to the penetration-depth dependence of mass  
299 accommodation and plausibly explained by different scenarios/combinations/ratios of volatility  
300 and diffusivity, which can lead to a substantial decrease of  $\alpha_{\text{eff}}$  relative to  $\alpha_s$  in semi-solid particles.  
301 With regard to the dependence of  $\alpha_{\text{eff}}$  on  $C^0$ , mixing effects and non-ideality may lead to deviations  
302 between  $C^0$  and  $C^*$  (Zuend and Seinfeld, 2012), which should be taken into account in further  
303 investigations of mass accommodation and its influence on the formation and growth of SOA  
304 particles.

305 On the other hand, high reactivity can compensate the influence of low diffusivity and mass  
306 transport limitations in the particle phase, keeping  $\alpha_{\text{eff}}$  close to  $\alpha_s$ . In case of non-reactive  
307 partitioning, the effective penetration depth used to calculate  $\alpha_{\text{eff}}$  is one fifth of the particle radius,  
308 i.e.,  $x_{\text{eff}}/r_p = 0.2$  (Eq. 6). In case of reactive uptake, however,  $x_{\text{eff}}$  decreases with increasing  
309 reactivity and with decreasing diffusivity according to Eqs. (7) to (9). Figure 5a illustrates how the  
310 effective penetration depth normalized by particle radius,  $x_{\text{eff}}/r_p$ , decreases with increasing first-



311 order bulk reaction rate coefficient,  $k_b$ , and with decreasing diffusion coefficient,  $D_b$ . The reduced  
312 effective penetration depths at high  $k_b$  and low  $D_b$  reflect that reactive uptake by semisolid particles  
313 proceeds mainly through chemical reaction near the surface (Shiraiwa et al., 2013a). Figure 5b  
314 illustrates how  $\alpha_{\text{eff}}$  depends on volatility and diffusivity for reactive uptake with  $\alpha_s = 1$  and a first-  
315 order bulk reaction rate coefficient  $k_b = 0.1 \text{ s}^{-1}$ . In comparison to Fig. 3b for non-reactive  
316 partitioning, Fig. 5b shows that particle phase reactivity leads to an extension of the volatility-  
317 diffusivity parameter space where  $\alpha_{\text{eff}} \approx \alpha_s$  (red area): For semi-solid particles with low diffusivity,  
318 the parameter range of strong deviations between  $\alpha_{\text{eff}}$  and  $\alpha_s$  (yellow/green/blue area) is shifted  
319 towards higher volatility (lower right corner).

320

### 321 **Summary and conclusions**

322 Traditional SOA modeling approaches are often using the Fuchs-Sutugin approximation of  
323 mass-transport kinetics at the gas-particle interface in combination with mass accommodation  
324 coefficients that are not appropriately defined, leading to inconsistent results and conclusions. To  
325 overcome such deficiencies and difficulties, we have introduced an effective mass accommodation  
326 coefficient  $\alpha_{\text{eff}}$  that depends on penetration depth and is a function of surface accommodation  
327 coefficient, volatility, bulk diffusivity, and particle-phase reaction rate coefficient. Application of  
328  $\alpha_{\text{eff}}$  in the traditional F-S approximation of SOA partitioning yields results that are consistent with  
329 detailed kinetic multilayer models (KM-GAP; Shiraiwa et al., 2012) and two-film models  
330 (MOSAIC, Zaveri et al., 2014)).

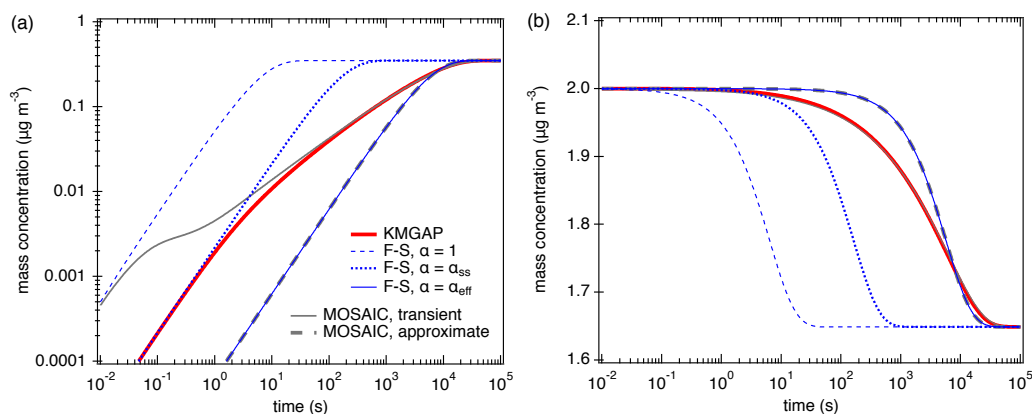
331 We suggest that  $\alpha_{\text{eff}}$  and its dependence on penetration depth and related parameters should  
332 be applied and considered when the F-S approximation is used to investigate and simulate gas-  
333 particle interactions in viscous or semi-solid organic aerosols. The simple parameterization can be  
334 incorporated into regional and global models for a more realistic representation of SOA processes  
335 in the atmosphere, which seems particularly important with regard to the ubiquity of amorphous  
336 semi-solid or glassy particles predicted for the free troposphere as well as planetary boundary layer  
337 air at low relative humidity and low temperature (Maclean et al., 2017; Shiraiwa et al., 2017).

338 In the analysis and interpretation of SOA chamber and laboratory experiments,  $\alpha_{\text{eff}}$   
339 provides a simple way of accounting for the potential impact of volatility, diffusivity, and particle  
340 phase state on the kinetics of gas-particle partitioning for analysis and interpretation of chamber  
341 experiments. In particular, it may help to address and resolve apparent inconsistencies between the



342 definitions and parameter values of mass accommodation coefficients that are derived from  
343 experimental data and from molecular dynamics simulations.

344         At short timescales, however,  $\alpha_{\text{eff}}$  is not sufficient to properly describe the kinetics of gas-  
345 particle interactions with the F-S approximation. Such conditions require detailed kinetic model  
346 simulations with kinetic multilayer models or equivalent approaches explicitly resolving mass  
347 transport at the surface and in the bulk of the particle. The same applies for particles with layered  
348 structures such as surface crusts (solid/viscous surface layers) that may form upon chemical aging  
349 and can strongly impact the uptake of semi-volatile compounds and multiphase chemical processes  
350 in the particle phase (Pfrang et al., 2011; Vander Wall et al., 2018; Zhou et al., 2019). Moreover,  
351 mixed organic-inorganic particles often undergo liquid-liquid phase separation at moderate and  
352 high RH (Krieger et al., 2012; You et al., 2014; Zuend and Seinfeld, 2012), and liquid-liquid phase  
353 separation can also occur for purely organic particles (Song et al., 2017). The interplay of particle  
354 phase state and phase separation can further impact SOA partitioning (Shiraiwa et al., 2013b). In  
355 such complex particle morphologies with multiple phases, gradients and discontinuities of  
356 diffusivity may occur within the particle bulk and require more advanced modeling approaches of  
357 gas-particle interaction kinetics to be addressed in future studies.

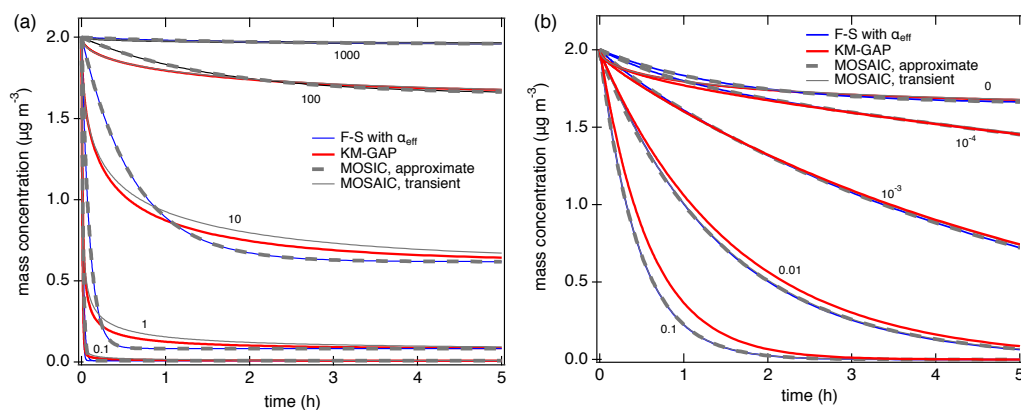


358

359

360 **Figure 1.** Temporal evolution of the particle phase concentration (a) and the gas phase  
361 concentration (b) of semi-volatile organic compounds (SVOC,  $C^0 = 100 \mu\text{g m}^{-3}$ ) interacting with  
362 semisolid seed aerosol particles ( $D_b = 10^{-15} \text{ cm}^2 \text{ s}^{-1}$ ,  $\omega = 2 \times 10^4 \text{ cm s}^{-1}$ ,  $\rho_p = 1 \text{ g cm}^{-3}$ ). The red lines  
363 are simulation results of KM-GAP, and the blue lines are the results of an aerosol dynamic model  
364 that employs the Fuchs-Sutugin approximation with  $\alpha = \alpha_s = 1$  (dashed),  $\alpha = \alpha_{ss} = 3 \times 10^{-2}$  (dotted),  
365 and  $\alpha = \alpha_{eff} = 8 \times 10^{-4}$  (solid). The gray lines represent the MOSAIC transient solution (solid) and  
366 approximate solution (dashed) (Zaveri et al., 2014).

367

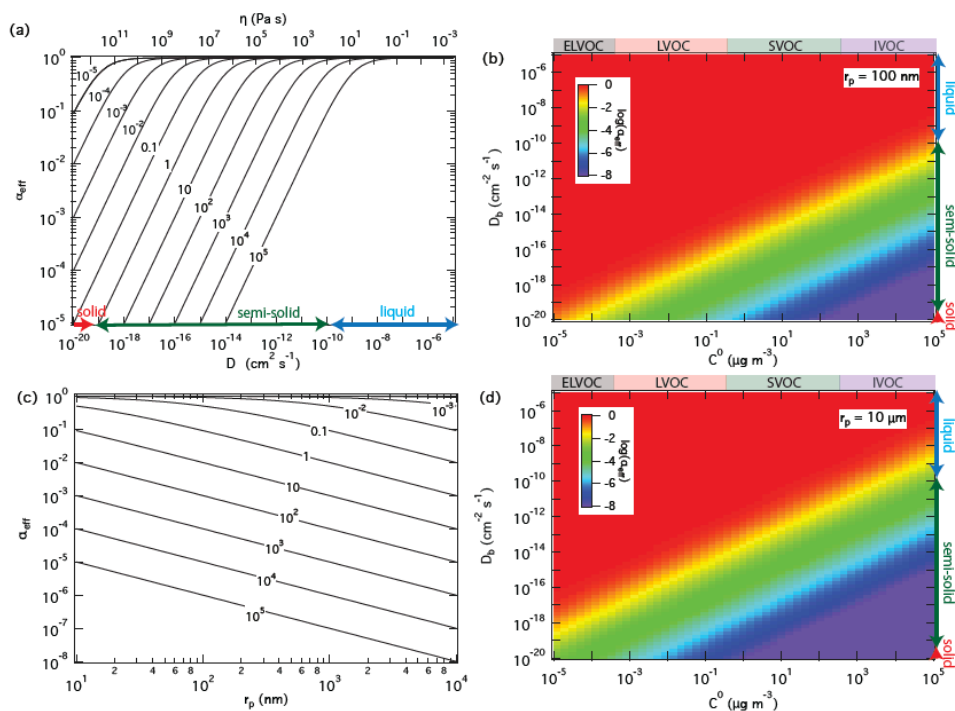


368

369

370 **Figure 2.** Temporal evolution of the gas phase concentration of organic compounds interacting  
371 with semisolid seed aerosol particles ( $\alpha_s = 1$ ,  $\omega = 2 \times 10^4 \text{ cm s}^{-1}$ ,  $D_b = 10^{-15} \text{ cm}^2 \text{ s}^{-1}$ ,  $\rho_p = 1 \text{ g cm}^{-3}$ ):  
372 (a) Non-reactive partitioning of compounds with different volatilities ( $C^0 = 0.1, 1, 10, 100, 1000$   
373  $\mu\text{g m}^{-3}$ ); (b) reactive uptake of semi-volatile compounds ( $C^0 = 100 \mu\text{g m}^{-3}$ ) with different first-  
374 order bulk reaction rate coefficients ( $k_b = 0, 10^{-4}, 10^{-3}, 0.01, 0.1 \text{ s}^{-1}$ ). The red lines are simulation  
375 results of KM-GAP, and the blue lines are the results of an aerosol dynamic model that employs  
376 the Fuchs-Sutugin approximation with  $\alpha_{\text{eff}} = \alpha(r_p/5)$  for non-reactive partitioning (a) and with  $\alpha_{\text{eff}}$   
377  $= \alpha(x_{\text{eff}})$  and  $x_{\text{eff}}$  from Eq. (5) for reactive uptake (b). The gray lines represent the MOSAIC  
378 transient solution (solid) and approximate solution (dashed) (Zaveri et al., 2014).

379



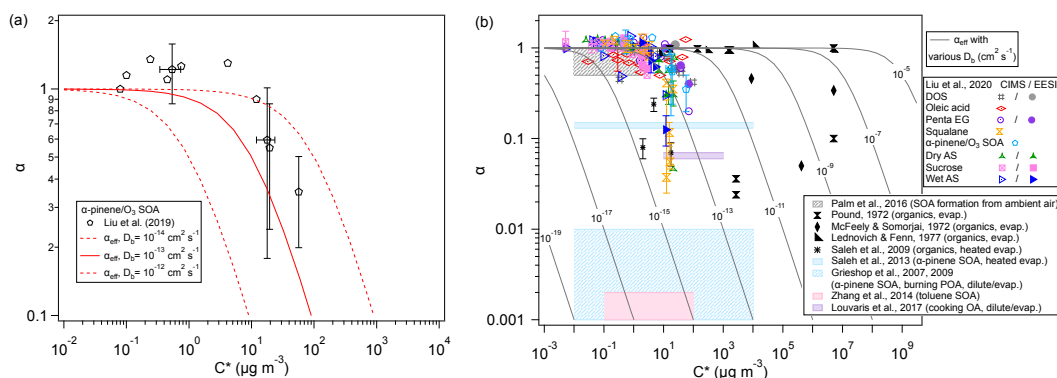
380

381

382 **Figure 3.** Effective mass accommodation coefficients,  $\alpha_{\text{eff}}$ , for non-reactive partitioning of organic  
 383 compounds  $Z$  ( $\alpha_s = 1$ ,  $\omega = 2 \times 10^4 \text{ cm s}^{-1}$ ) with liquid, semi-solid, or solid aerosol particles ( $\rho_p = 1$   
 384  $\text{g cm}^{-3}$ ) depending on pure compound volatility,  $C^0$ , particle bulk diffusivity,  $D_b$  (corresponding to  
 385 viscosity,  $\eta$ ), and particle radius,  $r_p$ :  $\alpha_{\text{eff}}$  calculated as a function of  $D_b$  for  $C^0 = 10^{-5}$  to  $10^5 \mu\text{g m}^{-3}$   
 386 with  $r_p = 100 \text{ nm}$  (a);  $\alpha_{\text{eff}}$  calculated as a function of  $C^0$  and  $D_b$  with  $r_p = 100 \text{ nm}$  (b) and  $10 \mu\text{m}$   
 387 (d);  $\alpha_{\text{eff}}$  calculated as a function of particle radius for  $D_b = 10^{-15} \text{ cm}^2 \text{ s}^{-1}$  and different levels of  
 388 volatility ( $C^0 = 10^{-3}$  to  $10^5 \mu\text{g m}^{-3}$ ) (c).

389





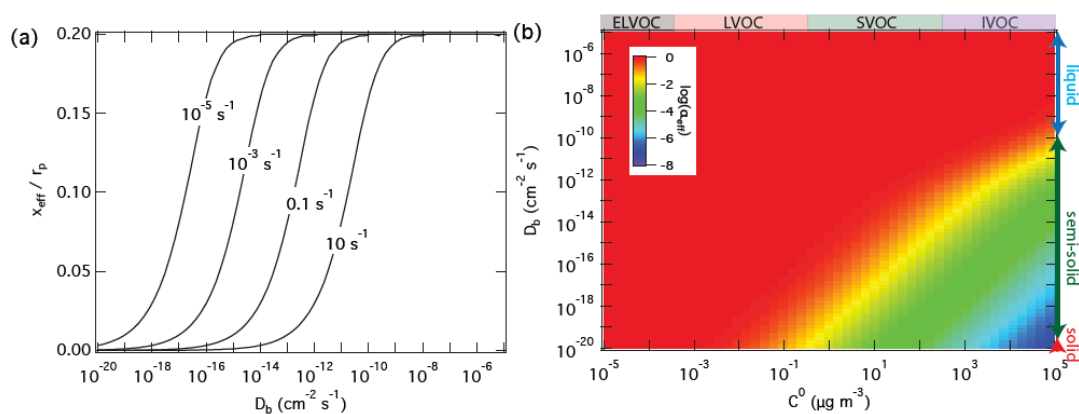
390  
 391

392 **Figure 4.** Effective mass accommodation coefficients,  $\alpha_{\text{eff}}$  (lines, Eqs. 5-10) compared to  
 393 measurement-derived mass accommodation coefficients,  $\alpha$  (data points/shaded areas, Eqs. 1-2),  
 394 plotted against effective saturation mass concentration,  $C^*$ , for various SOA and surrogate systems  
 395 assuming  $\alpha_s = 1$ ,  $\omega = 2 \times 10^4 \text{ cm s}^{-1}$ ,  $\rho = 1 \text{ g cm}^{-3}$ ,  $r_p = 100 \text{ nm}$ , and  $C^0 = C^*$ : (a) observational  
 396 results from laboratory experiments with semi-volatile components of SOA generated by  
 397 ozonolysis of  $\alpha$ -pinene (data points, (Liu et al., 2019)) compared to  $\alpha_{\text{eff}}$  for  $D_b = 10^{-14}$  to  $10^{-12} \text{ cm}^2$   
 398  $\text{s}^{-1}$  (lines); (b) observational results from earlier experimental investigations of laboratory-  
 399 generated and ambient samples (data points/shaded areas, compiled by Liu et al., 2019) compared  
 400 to generic values of  $\alpha_{\text{eff}}$  for  $D_b = 10^{-19}$  to  $10^{-5} \text{ cm}^2 \text{ s}^{-1}$  (lines).

401



402



403

404

405 **Figure 5.** Effective penetration depths normalized by particle radius,  $x_{\text{eff}}$ , and mass  
406 accommodation coefficients,  $\alpha_{\text{eff}}$ , for reactive uptake of organic compounds  $Z$  ( $\alpha_s = 1$ ,  $\omega = 2 \times 10^4$   
407  $\text{cm s}^{-1}$ ) by liquid, semi-solid, or solid aerosol particles ( $r_p = 100 \text{ nm}$ ,  $\rho_p = 1 \text{ g cm}^{-3}$ ) depending on  
408 pure compound volatility,  $C^0$ , particle bulk diffusivity  $D_b$ , and first-order bulk reaction rate  
409 coefficient,  $k_b$ : (a)  $x_{\text{eff}}$  calculated as a function of  $D_b$  and  $k_b = 10^{-5}$  to  $10 \text{ s}^{-1}$ ; (b)  $\alpha_{\text{eff}}$  calculated as a  
410 function of  $C^0$  and  $D_b$  for  $k_b = 0.1 \text{ s}^{-1}$ .

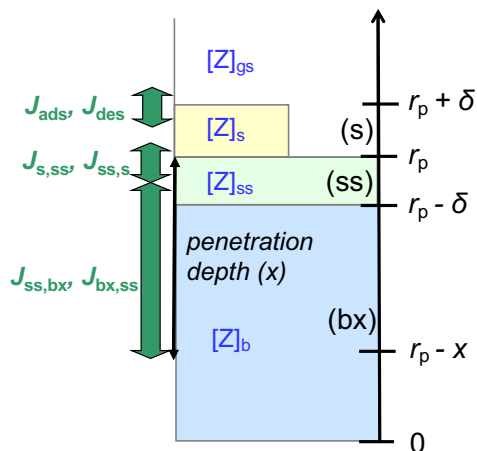
411

412



413 **Appendix:**

414 **Derivation of penetration-depth-dependent mass accommodation coefficient**



415

416 **Figure A1.** Schematic illustration of the kinetic multilayer modelling approach resolving mass  
 417 transport fluxes ( $J$ ) between the near-surface gas phase (gs), the sorption layer (s), the quasi-static  
 418 surface layer (ss), and the bulk layer at penetration depth  $x$  (bx) (Shiraiwa et al., 2012).

419

420 Figure A1 illustrates the applied kinetic multi-layer model framework, in which the  
 421 structure and composition of a particle are described by a sorption layer (s), a quasi-static surface  
 422 layer (ss), multiple bulk layers (b), and any volatile, semi-volatile, or low-volatile chemical species  
 423 ( $Z$ ) that can undergo gas-particle partitioning and transport between the different layers and  
 424 chemical reactions with each other (Pöschl et al., 2007; Shiraiwa et al., 2012). At low gas-phase  
 425 concentration levels or high surface bulk exchange rates (e.g., for liquid particles under dilute  
 426 atmospheric conditions), surface coverage and saturation effects can be neglected, and the surface  
 427 accommodation coefficient ( $\alpha_s$ ) approaches the parameter value for an adsorbate-free surface ( $\alpha_s$   
 428  $\approx \alpha_{s,0}$ ) (Pöschl et al., 2007; Shiraiwa et al., 2012). In the absence of condensed-phase reactions, a  
 429 quasi-static surface accommodation coefficient ( $\alpha_{ss}$ ), i.e. the probability for a gas molecule  
 430 colliding with the surface to enter the quasi-static surface layer, can be calculated as follows  
 431 (Shiraiwa et al., 2012):

432 
$$\alpha_{ss} = \alpha_s \frac{J_{s,ss}}{J_d + J_{s,ss}} = \alpha_s \frac{k_{s,ss}}{k_d + k_{s,ss}} \quad (\text{A1})$$



433 Here  $J_d$  is the desorption flux of Z and  $k_d$  is the corresponding first-order rate coefficient;  $J_{s,ss}$  and  
 434  $k_{s,ss}$  represent the flux and first-order rate coefficient of transfer between the sorption layer and the  
 435 quasi-static surface layer. The probability for an individual gas molecule colliding with the surface  
 436 to enter the bulk with a penetration depth  $x$  can be described by a penetration depth-dependent  
 437 mass accommodation coefficient,  $\alpha(x)$ , defined as follows:

$$438 \quad \alpha(x) = \alpha_{ss} \frac{\Psi_{ss,bx}}{1 - \Psi_{ss,s} \Psi_{s,ss}} \quad (A2)$$

439 Here  $\Psi_{s,ss}$  is the probability for Z in the sorption layer to enter the quasi-static surface layer and  
 440  $\Psi_{ss,bx}$  and  $\Psi_{ss,s}$  are the probabilities for Z in the quasi-static surface layer to enter the bulk with the  
 441 penetration depth of  $x$  or the sorption layer, respectively, which are determined by the  
 442 corresponding fluxes and first-order rate coefficients of mass transport (Shiraiwa et al., 2012):

$$443 \quad \Psi_{s,ss} = J_{s,ss} / (J_{s,ss} + J_{des}) = k_{s,ss} / (k_{s,ss} + k_d) \quad (A3)$$

$$444 \quad \Psi_{ss,s} = J_{ss,s} / (J_{ss,bx} + J_{ss,s}) = k_{ss,s} / (k_{ss,bx} + k_{ss,s}) \quad (A4)$$

$$445 \quad \Psi_{ss,bx} = J_{ss,bx} / (J_{ss,bx} + J_{ss,s}) = k_{ss,bx} / (k_{ss,bx} + k_{ss,s}) \quad (A5)$$

446 Inserting Eqs. (A3)-(A5) in Eq. (A2) leads to:

$$448 \quad \alpha(x) = \alpha_s \frac{k_{s,ss}}{k_d + k_{s,ss}} \frac{\frac{k_{ss,bx}}{k_{ss,bx} + k_{ss,s}}}{1 - \frac{k_{ss,s}}{k_{ss,bx} + k_{ss,s}} \cdot \frac{k_{s,ss}}{k_{s,ss} + k_d}}$$

$$449 \quad = \alpha_s \frac{k_{s,ss} k_{ss,bx}}{(k_d + k_{s,ss})(k_{ss,bx} + k_{ss,s}) \left(1 - \frac{k_{ss,s}}{k_{ss,bx} + k_{ss,s}} \cdot \frac{k_{s,ss}}{k_{s,ss} + k_d}\right)}$$

$$450 \quad = \alpha_s \frac{k_{s,ss} k_{ss,bx}}{(k_d + k_{s,ss})(k_{ss,bx} + k_{ss,s}) - k_{ss,s} k_{s,ss}}$$

$$451 \quad = \alpha_s \frac{k_{s,ss} k_{ss,bx}}{k_d k_{ss,bx} + k_{s,ss} k_{ss,bx} + k_d k_{ss,s}} = \alpha_s \frac{1}{1 + \frac{k_d k_{ss,s} + k_d k_{ss,bx}}{k_{s,ss} k_{ss,bx}}}$$

$$452 \quad = \alpha_s \frac{1}{1 + \frac{k_d}{k_{s,ss}} \frac{k_{ss,s} + k_{ss,bx}}{k_{ss,bx}}} = \alpha_s \frac{1}{1 + \frac{k_d}{k_{s,ss}} \left(1 + \frac{k_{ss,s}}{k_{ss,bx}}\right)} \quad (A6)$$

453 The first-order rate coefficients of adsorption and desorption are given by  $k_a = \alpha_s \omega / 4$  and  $k_d =$   
 454  $1/\tau_d$ , respectively, where  $\omega$  ( $\text{cm s}^{-1}$ ) is the mean thermal velocity of Z in the gas phase and  $\tau_d$  is the  
 455 lifetime of desorption from the sorption layer (Pöschl et al., 2007; Shiraiwa et al., 2012). The rate



456 coefficient of mass transfer between sorption layer and quasi-static surface layer can be estimated  
457 based on the Fick's first law of diffusion considering that a molecule in the sorption layer needs to  
458 travel a distance of  $\delta$  to move into the quasi-static surface layer:  $k_{s,s} \approx D_b / \delta^2$  (Shiraiwa et al.,  
459 2012). An estimate for  $k_{s,s}$  can be determined considering mass transport under equilibrium  
460 conditions, where mass balance implies  $J_{s,ss} = J_{ss,s}$ , i.e.,  $k_{s,ss} [Z]_{s,eq} = k_{ss,s} [Z]_{ss,eq}$ , and  $J_{des} = J_{ads}$ , i.e.,  
461  $k_d [Z]_{s,eq} = k_a [Z]_{g,eq}$  (Shiraiwa et al., 2012). Here  $[Z]_{g,eq}$ ,  $[Z]_{s,eq}$ , and  $[Z]_{ss,eq}$  are the equilibrium or  
462 solubility saturation number concentrations of Z in the gas phase, on the sorption layer, and in the  
463 quasi-static surface layer, respectively:

$$464 \quad k_{s,ss} = k_{ss,s} \frac{k_d [Z]_{ss,eq}}{k_a [Z]_{g,eq}} \quad (A7)$$

$$465 \quad \frac{k_d}{k_{s,ss}} = \frac{k_a [Z]_{g,eq}}{k_{ss,s} [Z]_{ss,eq}} = \frac{k_a [Z]_{g,eq}}{k_{ss,s} [Z]_{b,eq} \delta} \quad (A8)$$

466

467 In analogy, the first-order rate coefficient  $k_{bx,ss}$  can be estimated based on the Fick's first law of  
468 diffusion, considering that a molecule Z at penetration depth  $x$  in the bulk needs to travel a distance  
469 of  $x - \delta$  to move into the quasi-static surface layer (Fig. A1):  $k_{bx,ss} \approx D_b / (x - \delta)$ . Under equilibrium  
470 conditions,  $J_{ss,bx} = J_{bx,ss}$  and  $k_{ss,bx} [Z]_{ss,eq} = k_{bx,ss} [Z]_{b,eq}$  which leads to  $k_{ss,bx} = k_{bx,ss} / \delta = D_b / (\delta(x - \delta))$   
471 assuming ideal mixing conditions and  $[Z]_{b,eq} = [Z]_{ss,eq} / \delta$  (Shiraiwa et al., 2012). Thus,  $k_{ss,s} / k_{ss,bx} =$   
472  $(D_b / \delta^2) / (D_b / (\delta(x - \delta))) = (x - \delta) / \delta$ .

473 Based on the absorptive partitioning theory (Donahue et al., 2006; Pankow, 1994),

474

$$475 \quad C^0 = \frac{C^g}{C^p} C_{OA} \quad (A9)$$

476 where  $C^0$  ( $\mu\text{g m}^{-3}$ ) is the pure compound saturation mass concentration,  $C^g$  and  $C^p$  ( $\mu\text{g m}^{-3}$ ) are the  
477 gas-phase and particle-phase mass concentrations of the compound Z, respectively, and  $C_{OA}$  ( $\mu\text{g}$   
478  $\text{m}^{-3}$ ) is the total organic aerosol mass concentration.  $C^g$  and  $[Z]_{g,eq}$  are related through the following  
479 equation:

$$480 \quad C^g = \frac{[Z]_{g,eq} M}{N_A} \cdot 10^{12} \frac{\mu\text{g m}^{-3}}{\text{g cm}^{-3}} \quad (A10)$$

481 where  $M$  is the molar mass of compound Z.  $[Z]_{g,eq}$  is the equilibrium (saturation) number  
482 concentration of Z in the gas phase.  $[Z]_{g,eq}$  can be calculated using the saturation vapor pressure  $p$ :



483  $[Z]_{g,eq} = p N_A / (R T)$  where  $N_A$  is the Avogadro number,  $R$  is the gas constant, and  $T$  is the  
484 temperature.  $[Z]_{b,eq}$  corresponds to the ratio between the number concentration of  $Z$  in the particle  
485 phase (per  $m^3$  of air) to the particle volume concentration ( $m^3$  per  $m^3$  of air), which can be  
486 expressed using  $C_Z^{PM}$  and  $C_{OA}$  with the particle density  $\rho_P$  ( $g\ cm^{-3}$ ):

$$487 \quad [Z]_{b,eq} = \frac{C^P}{\rho} \frac{N_A}{C_{OA} M} = \frac{C^P N_A \rho_P}{C_{OA} M} \quad (A11)$$

488 Combining Eq. (A9) – (A11) would lead to:

$$489 \quad \frac{[Z]_{g,eq}}{[Z]_{b,eq}} = \frac{\frac{C^g N_A}{M} \cdot 10^{-12}}{\frac{C^P N_A \rho_P}{C_{OA} M}} = \frac{C^g}{C^P} \frac{C_{OA}}{\rho_P} \frac{1}{\rho_P} \cdot 10^{-12} = \frac{C^0}{\rho_P} \cdot 10^{-12} \frac{g\ cm^{-3}}{\mu g\ m^{-3}} \quad (A12)$$

490 Inserting Eq. (A8) into Eq. (A6) and combination with Eq. (A12) leads to:

$$491 \quad \alpha(x) = \alpha_s \frac{1}{1 + \frac{k_a}{k_{ss,s}} \frac{[Z]_{g,eq}}{[Z]_{b,eq}} \delta \left(1 + \frac{x - \delta}{\delta}\right)} = \alpha_s \frac{1}{1 + \frac{\alpha_s \omega C^0}{4 D_b \rho_P} x \cdot 10^{-12} \frac{g\ cm^{-3}}{\mu g\ m^{-3}}} \quad (A13)$$

492

493 **Acknowledgements.** MS acknowledges funding by the National Science Foundation (AGS-  
494 1654104) and the Department of Energy (DE-SC0018349). We thank Jose Jimenez (CU Boulder)  
495 for stimulating discussions and for sharing published data and experimental information as  
496 presented in Figure 4.

497

498 **Author contributions.** MS and UP designed the study, analyzed the data, and wrote the paper.  
499 MS conducted kinetic modeling.

500

501 **Competing interests.** The authors declare that they have no conflict of interest.

502

503 **Data availability.** The simulation data may be obtained from the corresponding author upon  
504 request.

505

506 **References.**

507 Alpert, P. A., Corral Arroyo, P., Dou, J., Krieger, U. K., Steimer, S. S., Förster, J.-D., Ditas, F.,  
508 Pöhlker, C., Rossignol, S., Passananti, M., Perrier, S., George, C., Shiraiwa, M., Berkemeier, T.,



- 509 Watts, B. and Ammann, M.: Visualizing reaction and diffusion in xanthan gum aerosol particles  
510 exposed to ozone, *Phys. Chem. Chem. Phys.*, 21, 20613-20627, 10.1039/C9CP03731D, 2019.
- 511 Aumont, B., Szopa, S. and Madronich, S.: Modelling the evolution of organic carbon during its  
512 gas-phase tropospheric oxidation: development of an explicit model based on a self generating  
513 approach, *Atmos. Chem. Phys.*, 5, 2497-2517, 10.5194/acp-5-2497-2005, 2005.
- 514 Berkemeier, T., Steimer, S., Krieger, U. K., Peter, T., Poschl, U., Ammann, M. and Shiraiwa, M.:  
515 Ozone uptake on glassy, semi-solid and liquid organic matter and the role of reactive oxygen  
516 intermediates in atmospheric aerosol chemistry, *Phys. Chem. Chem. Phys.*, 18, 12662-12674,  
517 10.1039/C6CP00634E, 2016.
- 518 Berkemeier, T., Ammann, M., Krieger, U. K., Peter, T., Spichtinger, P., Pöschl, U., Shiraiwa, M.  
519 and Huisman, A. J.: Technical note: Monte Carlo genetic algorithm (MCGA) for model analysis  
520 of multiphase chemical kinetics to determine transport and reaction rate coefficients using multiple  
521 experimental data sets, *Atmos. Chem. Phys.*, 17, 8021-8029, 10.5194/acp-17-8021-2017, 2017.
- 522 Cappa, C. D., Jathar, S. H., Kleeman, M. J., Docherty, K. S., Jimenez, J. L., Seinfeld, J. H. and  
523 Wexler, A. S.: Simulating secondary organic aerosol in a regional air quality model using the  
524 statistical oxidation model - Part 2: Assessing the influence of vapor wall losses, *Atmos. Chem.  
525 Phys.*, 16, 3041-3059, 10.5194/acp-16-3041-2016, 2016.
- 526 Davies, J. F. and Wilson, K. R.: Nanoscale interfacial gradients formed by the reactive uptake of  
527 OH radicals onto viscous aerosol surfaces, *Chem. Sci.*, 6, 7020-7027, 2015.
- 528 Donahue, N. M., Robinson, A. L., Stanier, C. O. and Pandis, S. N.: Coupled partitioning, dilution,  
529 and chemical aging of semivolatile organics, *Environ. Sci. Technol.*, 40, 2635-2643,  
530 10.1021/es052297c, 2006.
- 531 Fowler, K., Connolly, P. J., Topping, D. O. and O'Meara, S.: Maxwell–Stefan diffusion: a  
532 framework for predicting condensed phase diffusion and phase separation in atmospheric aerosol,  
533 *Atmos. Chem. Phys.*, 18, 1629-1642, 10.5194/acp-18-1629-2018, 2018.
- 534 Jathar, S. H., Cappa, C. D., Wexler, A. S., Seinfeld, J. H. and Kleeman, M. J.: Simulating  
535 secondary organic aerosol in a regional air quality model using the statistical oxidation model -  
536 Part 1: Assessing the influence of constrained multi-generational ageing, *Atmos. Chem. Phys.*, 16,  
537 2309-2322, 10.5194/acp-16-2309-2016, 2016.
- 538 Jimenez, J. L., Canagaratna, M. R., Donahue, N. M., Prevot, A. S. H., Zhang, Q., Kroll, J. H.,  
539 DeCarlo, P. F., Allan, J. D., Coe, H., Ng, N. L., Aiken, A. C., Docherty, K. S., Ulbrich, I. M.,  
540 Grieshop, A. P., Robinson, A. L., Duplissy, J., Smith, J. D., Wilson, K. R., Lanz, V. A., Hueglin,  
541 C., Sun, Y. L., Tian, J., Laaksonen, A., Raatikainen, T., Rautiainen, J., Vaattovaara, P., Ehn, M.,  
542 Kulmala, M., Tomlinson, J. M., Collins, D. R., Cubison, M. J., Dunlea, E. J., Huffman, J. A.,  
543 Onasch, T. B., Alfarra, M. R., Williams, P. I., Bower, K., Kondo, Y., Schneider, J., Drewnick, F.,  
544 Borrmann, S., Weimer, S., Demerjian, K., Salcedo, D., Cottrell, L., Griffin, R., Takami, A.,  
545 Miyoshi, T., Hatakeyama, S., Shimono, A., Sun, J. Y., Zhang, Y. M., Dzepina, K., Kimmel, J. R.,  
546 Sueper, D., Jayne, J. T., Herndon, S. C., Trimborn, A. M., Williams, L. R., Wood, E. C.,



- 547 Middlebrook, A. M., Kolb, C. E., Baltensperger, U. and Worsnop, D. R.: Evolution of organic  
548 aerosols in the atmosphere, *Science*, 326, 1525-1529, 10.1126/science.1180353, 2009.
- 549 Julin, J., Winkler, P. M., Donahue, N. M., Wagner, P. E. and Riipinen, I. A.: Near unity mass  
550 accommodation coefficient of organic molecules of varying structure, *Environ. Sci. Technol.*, 48,  
551 12083–12089, 10.1021/es501816h, 2014.
- 552 Kanakidou, M., Seinfeld, J. H., Pandis, S. N., Barnes, I., Dentener, F. J., Facchini, M. C., Van  
553 Dingenen, R., Ervens, B., Nenes, A., Nielsen, C. J., Swietlicki, E., Putaud, J. P., Balkanski, Y.,  
554 Fuzzi, S., Horth, J., Moortgat, G. K., Winterhalter, R., Myhre, C. E. L., Tsigaridis, K., Vignati, E.,  
555 Stephanou, E. G. and Wilson, J.: Organic aerosol and global climate modelling: a review, *Atmos.*  
556 *Chem. Phys.*, 5, 1053-1123, 2005.
- 557 Knopf, D. A., Alpert, P. A. and Wang, B.: The Role of Organic Aerosol in Atmospheric Ice  
558 Nucleation: A Review, *ACS Earth Space Chem.*, 10.1021/acsearthspacechem.7b00120, 2018.
- 559 Kolb, C. E., Cox, R. A., Abbatt, J. P. D., Ammann, M., Davis, E. J., Donaldson, D. J., Garrett, B.  
560 C., George, C., Griffiths, P. T., Hanson, D. R., Kulmala, M., McFiggans, G., Pöschl, U., Riipinen,  
561 I., Rossi, M. J., Rudich, Y., Wagner, P. E., Winkler, P. M., Worsnop, D. R. and O' Dowd, C. D.:  
562 An overview of current issues in the uptake of atmospheric trace gases by aerosols and clouds,  
563 *Atmos. Chem. Phys.*, 10, 10561-10605, 10.5194/acp-10-10561-2010, 2010.
- 564 Koop, T., Bookhold, J., Shiraiwa, M. and Pöschl, U.: Glass transition and phase state of organic  
565 compounds: dependency on molecular properties and implications for secondary organic aerosols  
566 in the atmosphere, *Phys. Chem. Chem. Phys.*, 13, 19238-19255, 2011.
- 567 Kostenidou, E., Karnezi, E., Hite Jr, J. R., Bougiatioti, A., Cerully, K., Xu, L., Ng, N. L., Nenes,  
568 A. and Pandis, S. N.: Organic aerosol in the summertime southeastern United States: components  
569 and their link to volatility distribution, oxidation state and hygroscopicity, *Atmos. Chem. Phys.*,  
570 18, 5799-5819, 10.5194/acp-18-5799-2018, 2018.
- 571 Krapf, M., El Haddad, I., Bruns, Emily A., Molteni, U., Daellenbach, Kaspar R., Prévôt, André S.  
572 H., Baltensperger, U. and Dommen, J.: Labile Peroxides in Secondary Organic Aerosol, *Chem*, 1,  
573 603-616, 2016.
- 574 Krieger, U. K., Marcolli, C. and Reid, J. P.: Exploring the complexity of aerosol particle properties  
575 and processes using single particle techniques, *Chem. Soc. Rev.*, 41, 6631-6662,  
576 10.1039/c2cs35082c, 2012.
- 577 Kroll, J. H. and Seinfeld, J. H.: Chemistry of secondary organic aerosol: Formation and evolution  
578 of low-volatility organics in the atmosphere, *Atmos. Environ.*, 42, 3593-3624,  
579 10.1016/j.atmosenv.2008.01.003, 2008.
- 580 Kuwata, M. and Martin, S. T.: Phase of atmospheric secondary organic material affects its  
581 reactivity, *Proc. Natl. Acad. Sci. U.S.A.*, 109, 17354-17359, 10.1073/pnas.1209071109, 2012.
- 582 Lee, B. H., Kostenidou, E., Hildebrandt, L., Riipinen, I., Engelhart, G. J., Mohr, C., DeCarlo, P.  
583 F., Mihalopoulos, N., Prevot, A. S. H., Baltensperger, U. and Pandis, S. N.: Measurement of the





- 584 ambient organic aerosol volatility distribution: application during the Finokalia Aerosol  
585 Measurement Experiment (FAME-2008), *Atmos. Chem. Phys.*, 10, 12149-12160, 10.5194/acp-  
586 10-12149-2010, 2010.
- 587 Li, Y. and Shiraiwa, M.: Timescales of secondary organic aerosols to reach equilibrium at various  
588 temperatures and relative humidities, *Atmos. Chem. Phys.*, 19, 5959-5971, 10.5194/acp-19-5959-  
589 2019, 2019.
- 590 Liu, P., Li, Y. J., Wang, Y., Gilles, M. K., Zaveri, R. A., Bertram, A. K. and Martin, S. T.: Lability  
591 of secondary organic particulate matter, *Proc. Natl. Acad. Sci. U.S.A.*, 113, 12643-12648, 2016.
- 592 Liu, X., Day, D. A., Krechmer, J. E., Brown, W., Peng, Z., Ziemann, P. J. and Jimenez, J. L.:  
593 Direct measurements of semi-volatile organic compound dynamics show near-unity mass  
594 accommodation coefficients for diverse aerosols, *Commun. Chem.*, 2, 98, 10.1038/s42004-019-  
595 0200-x, 2019.
- 596 Maclean, A. M., Butenhoff, C. L., Grayson, J. W., Barsanti, K., Jimenez, J. L. and Bertram, A. K.:  
597 Mixing times of organic molecules within secondary organic aerosol particles: a global planetary  
598 boundary layer perspective, *Atmos. Chem. Phys.*, 17, 13037-13048, 10.5194/acp-17-13037-2017,  
599 2017.
- 600 McVay, R. C., Cappa, C. D. and Seinfeld, J. H.: Vapor–Wall Deposition in Chambers: Theoretical  
601 Considerations, *Environ. Sci. Technol.*, 48, 10251-10258, 2014.
- 602 Mu, Q., Shiraiwa, M., Octaviani, M., Ma, N., Ding, A., Su, H., Lammel, G., Pöschl, U. and Cheng,  
603 Y.: Temperature effect on phase state and reactivity controls atmospheric multiphase chemistry  
604 and transport of PAHs, *Science Advances*, 4, eaap7314, 2018.
- 605 Pandis, S. N., Wexler, A. S. and Seinfeld, J. H.: Secondary organic aerosol formation and  
606 transport. 2. Predicting the ambient secondary organic aerosol - size distribution, *Atmos. Environ.*,  
607 27A, 2403-2416, 10.1016/0960-1686(93)90408-q, 1993.
- 608 Pankow, J. F.: An absorption model of gas-particle partitioning of organic-compounds in the  
609 atmosphere, *Atmos. Environ.*, 28, 185-188, 1994.
- 610 Perraud, V., Bruns, E. A., Ezell, M. J., Johnson, S. N., Yu, Y., Alexander, M. L., Zelenyuk, A.,  
611 Imre, D., Chang, W. L., Dabdub, D., Pankow, J. F. and Finlayson-Pitts, B. J.: Nonequilibrium  
612 atmospheric secondary organic aerosol formation and growth, *Proc. Natl. Acad. Sci. U.S.A.*, 109,  
613 2836-2841, 10.1073/pnas.1119909109, 2012.
- 614 Pfrang, C., Shiraiwa, M. and Pöschl, U.: Chemical ageing and transformation of diffusivity in  
615 semi-solid multi-component organic aerosol particles, *Atmos. Chem. Phys.*, 11, 7343-7354,  
616 10.5194/acp-11-7343-2011, 2011.
- 617 Pöschl, U., Rudich, Y. and Ammann, M.: Kinetic model framework for aerosol and cloud surface  
618 chemistry and gas-particle interactions - Part 1: General equations, parameters, and terminology,  
619 *Atmos. Chem. Phys.*, 7, 5989-6023, 2007.



- 620 Pöschl, U. and Shiraiwa, M.: Multiphase Chemistry at the Atmosphere–Biosphere Interface  
621 Influencing Climate and Public Health in the Anthropocene, *Chem. Rev.*, 115, 4440–4475,  
622 10.1021/cr500487s, 2015.
- 623 Pospisilova, V., Lopez-Hilfiker, F. D., Bell, D. M., El Haddad, I., Mohr, C., Huang, W., Heikkinen,  
624 L., Xiao, M., Dommen, J., Prevot, A. S. H., Baltensperger, U. and Slowik, J. G.: On the fate of  
625 oxygenated organic molecules in atmospheric aerosol particles, *Science Advances*, 6, eaax8922,  
626 10.1126/sciadv.aax8922, 2020.
- 627 Reid, J. P., Bertram, A. K., Topping, D. O., Laskin, A., Martin, S. T., Petters, M. D., Pope, F. D.  
628 and Rovelli, G.: The viscosity of atmospherically relevant organic particles, *Nat. Commun.*, 9,  
629 956, 10.1038/s41467-018-03027-z, 2018.
- 630 Riipinen, I., Pierce, J. R., Yli-Juuti, T., Nieminen, T., Hakkinen, S., Ehn, M., Junninen, H.,  
631 Lehtipalo, K., Petaja, T., Slowik, J., Chang, R., Shantz, N. C., Abbatt, J., Leaitch, W. R., Kerminen,  
632 V. M., Worsnop, D. R., Pandis, S. N., Donahue, N. M. and Kulmala, M.: Organic condensation: a  
633 vital link connecting aerosol formation to cloud condensation nuclei (CCN) concentrations,  
634 *Atmos. Chem. Phys.*, 11, 3865–3878, 10.5194/acp-11-3865-2011, 2011.
- 635 Roldin, P., Eriksson, A. C., Nordin, E. Z., Hermansson, E., Mogensen, D., Rusanen, A., Boy, M.,  
636 Swietlicki, E., Svenningsson, B., Zelenyuk, A. and Pagels, J.: Modelling non-equilibrium  
637 secondary organic aerosol formation and evaporation with the aerosol dynamics, gas- and particle-  
638 phase chemistry kinetic multilayer model ADCHAM, *Atmos. Chem. Phys.*, 14, 7953–7993,  
639 10.5194/acp-14-7953-2014, 2014.
- 640 Saleh, R., Shihadeh, A. and Khlystov, A.: On transport phenomena and equilibration time scales  
641 in thermodenuders, *Atmos. Meas. Tech.*, 4, 571–581, 10.5194/amt-4-571-2011, 2011.
- 642 Seinfeld, J. H. and Pandis, S. N.: *Atmospheric chemistry and physics: from air pollution to climate*  
643 *change*, John Wiley & Sons, 2016.
- 644 Shiraiwa, M., Ammann, M., Koop, T. and Pöschl, U.: Gas uptake and chemical aging of semisolid  
645 organic aerosol particles, *Proc. Natl. Acad. Sci. U.S.A.*, 108, 11003–11008,  
646 10.1073/pnas.1103045108, 2011.
- 647 Shiraiwa, M., Pfrang, C., Koop, T. and Pöschl, U.: Kinetic multi-layer model of gas-particle  
648 interactions in aerosols and clouds (KM-GAP): linking condensation, evaporation and chemical  
649 reactions of organics, oxidants and water, *Atmos. Chem. Phys.*, 12, 2777–2794, 10.5194/acp-12-  
650 2777-2012, 2012.
- 651 Shiraiwa, M. and Seinfeld, J. H.: Equilibration timescale of atmospheric secondary organic aerosol  
652 partitioning, *Geophys. Res. Lett.*, 39, L24801, 10.1029/2012GL054008, 2012.
- 653 Shiraiwa, M., Yee, L. D., Schilling, K. A., Loza, C. L., Craven, J. S., Zuend, A., Ziemann, P. J.  
654 and Seinfeld, J. H.: Size distribution dynamics reveal particle-phase chemistry in organic aerosol  
655 formation, *Proc. Natl. Acad. Sci. U.S.A.*, 110, 11746–11750, 10.1073/pnas.1307501110, 2013a.



- 656 Shiraiwa, M., Zuend, A., Bertram, A. K. and Seinfeld, J. H.: Gas-particle partitioning of  
657 atmospheric aerosols: interplay of physical state, non-ideal mixing and morphology, *Phys. Chem.*  
658 *Chem. Phys.*, 15, 11441-11453, 10.1039/C3CP51595H, 2013b.
- 659 Shiraiwa, M., Berkemeier, T., Schilling-Fahnestock, K. A., Seinfeld, J. H. and Pöschl, U.:  
660 Molecular corridors and kinetic regimes in the multiphase chemical evolution of secondary organic  
661 aerosol, *Atmos. Chem. Phys.*, 14, 8323-8341, 10.5194/acp-14-8323-2014, 2014.
- 662 Shiraiwa, M., Li, Y., Tsimpidi, A. P., Karydis, V. A., Berkemeier, T., Pandis, S. N., Lelieveld, J.,  
663 Koop, T. and Pöschl, U.: Global distribution of particle phase state in atmospheric secondary  
664 organic aerosols, *Nat. Commun.*, 8, 15002, 10.1038/ncomms15002, 2017.
- 665 Shrivastava, M., Cappa, C. D., Fan, J., Goldstein, A. H., Guenther, A. B., Jimenez, J. L., Kuang,  
666 C., Laskin, A., Martin, S. T., Ng, N. L., Petaja, T., Pierce, J. R., Rasch, P. J., Roldin, P., Seinfeld,  
667 J. H., Shilling, J., Smith, J. N., Thornton, J. A., Volkamer, R., Wang, J., Worsnop, D. R., Zaveri,  
668 R. A., Zelenyuk, A. and Zhang, Q.: Recent advances in understanding secondary organic aerosol:  
669 Implications for global climate forcing, *Rev. Geophys.*, 55, 509-559, 10.1002/2016RG000540,  
670 2017a.
- 671 Shrivastava, M., Lou, S., Zelenyuk, A., Easter, R. C., Corley, R. A., Thrall, B. D., Rasch, P. J.,  
672 Fast, J. D., Massey Simonich, S. L., Shen, H. and Tao, S.: Global long-range transport and lung  
673 cancer risk from polycyclic aromatic hydrocarbons shielded by coatings of organic aerosol, *Proc.*  
674 *Natl. Acad. Sci. U.S.A.*, 114, 1246-1251, 2017b.
- 675 Slade, J. H., Shiraiwa, M., Arangio, A., Su, H., Pöschl, U., Wang, J. and Knopf, D. A.: Cloud  
676 droplet activation through oxidation of organic aerosol influenced by temperature and particle  
677 phase state, *Geophys. Res. Lett.*, 44, 1583-1591, 10.1002/2016GL072424, 2017.
- 678 Song, M., Liu, P., Martin, S. T. and Bertram, A. K.: Liquid-liquid phase separation in particles  
679 containing secondary organic material free of inorganic salts, *Atmos. Chem. Phys.*, 17, 11261-  
680 11271, 10.5194/acp-17-11261-2017, 2017.
- 681 Tong, H., Arangio, A. M., Lakey, P. S. J., Berkemeier, T., Liu, F., Kampf, C. J., Brune, W. H.,  
682 Pöschl, U. and Shiraiwa, M.: Hydroxyl radicals from secondary organic aerosol decomposition in  
683 water, *Atmos. Chem. Phys.*, 16, 1761-1771, doi:10.5194/acp-16-1761-2016, 2016.
- 684 Tong, H., Zhang, Y., Filippi, A., Wang, T., Li, C., Liu, F., Leppla, D., Kourtchev, I., Wang, K.,  
685 Keskinen, H.-M., Levula, J. T., Arangio, A. M., Shen, F., Ditas, F., Martin, S. T., Artaxo, P.,  
686 Godoi, R. H. M., Yamamoto, C. I., de Souza, R. A. F., Huang, R.-J., Berkemeier, T., Wang, Y.,  
687 Su, H., Cheng, Y., Pope, F. D., Fu, P., Yao, M., Pöhlker, C., Petäjä, T., Kulmala, M., Andreae, M.  
688 O., Shiraiwa, M., Pöschl, U., Hoffmann, T. and Kalberer, M.: Radical Formation by Fine  
689 Particulate Matter Associated with Highly Oxygenated Molecules, *Environ. Sci. Technol.*, 53,  
690 12506-12518, 10.1021/acs.est.9b05149, 2019.
- 691 Tröstl, J., Chuang, W. K., Gordon, H., Heinritzi, M., Yan, C., Molteni, U., Ahlm, L., Frege, C.,  
692 Bianchi, F., Wagner, R., Simon, M., Lehtipalo, K., Williamson, C., Craven, J. S., Duplissy, J.,  
693 Adamov, A., Almeida, J., Bernhammer, A.-K., Breitenlechner, M., Brilke, S., Dias, A., Ehrhart,  
694 S., Flagan, R. C., Franchin, A., Fuchs, C., Guida, R., Gysel, M., Hansel, A., Hoyle, C. R., Jokinen,



- 695 T., Junninen, H., Kangasluoma, J., Keskinen, H., Kim, J., Krapf, M., Kürten, A., Laaksonen, A.,  
696 Lawler, M., Leiminger, M., Mathot, S., Möhler, O., Nieminen, T., Onnela, A., Petäjä, T., Piel, F.  
697 M., Miettinen, P., Rissanen, M. P., Rondo, L., Sarnela, N., Schobesberger, S., Sengupta, K., Sipilä,  
698 M., Smith, J. N., Steiner, G., Tomè, A., Virtanen, A., Wagner, A. C., Weingartner, E., Wimmer,  
699 D., Winkler, P. M., Ye, P., Carslaw, K. S., Curtius, J., Dommen, J., Kirkby, J., Kulmala, M.,  
700 Riipinen, I., Worsnop, D. R., Donahue, N. M. and Baltensperger, U.: The role of low-volatility  
701 organic compounds in initial particle growth in the atmosphere, *Nature*, 533, 527-531,  
702 10.1038/nature18271, 2016.
- 703 Trump, E. R. and Donahue, N. M.: Oligomer formation within secondary organic aerosols:  
704 equilibrium and dynamic considerations, *Atmos. Chem. Phys.*, 14, 3691-3701, 10.5194/acp-14-  
705 3691-2014, 2014.
- 706 Trump, E. R., Riipinen, I. and Donahue, N. M.: Interactions between atmospheric ultrafine  
707 particles and secondary organic aerosol mass: a model study, 2014.
- 708 Tsigaridis, K., Daskalakis, N., Kanakidou, M., Adams, P. J., Artaxo, P., Bahadur, R., Balkanski,  
709 Y., Bauer, S. E., Bellouin, N., Benedetti, A., Bergman, T., Berntsen, T. K., Beukes, J. P., Bian, H.,  
710 Carslaw, K. S., Chin, M., Curci, G., Diehl, T., Easter, R. C., Ghan, S. J., Gong, S. L., Hodzic, A.,  
711 Hoyle, C. R., Iversen, T., Jathar, S., Jimenez, J. L., Kaiser, J. W., Kirkevåg, A., Koch, D., Kokkola,  
712 H., Lee, Y. H., Lin, G., Liu, X., Luo, G., Ma, X., Mann, G. W., Mihalopoulos, N., Morcrette, J. J.,  
713 Müller, J. F., Myhre, G., Myriokefalitakis, S., Ng, N. L., O'Donnell, D., Penner, J. E., Pozzoli, L.,  
714 Pringle, K. J., Russell, L. M., Schulz, M., Sciare, J., Seland, Ø., Shindell, D. T., Sillman, S., Skeie,  
715 R. B., Spracklen, D., Stavrakou, T., Steenrod, S. D., Takemura, T., Tiitta, P., Tilmes, S., Tost, H.,  
716 van Noije, T., van Zyl, P. G., von Salzen, K., Yu, F., Wang, Z., Wang, Z., Zaveri, R. A., Zhang,  
717 H., Zhang, K., Zhang, Q. and Zhang, X.: The AeroCom evaluation and intercomparison of organic  
718 aerosol in global models, *Atmos. Chem. Phys.*, 14, 10845-10895, 10.5194/acp-14-10845-2014,  
719 2014.
- 720 Vaden, T. D., Imre, D., Beranek, J., Shrivastava, M. and Zelenyuk, A.: Evaporation kinetics and  
721 phase of laboratory and ambient secondary organic aerosol, *Proc. Natl. Acad. Sci. U.S.A.*, 108,  
722 2190-2195, 10.1073/pnas.1013391108, 2011.
- 723 Vander Wall, A. C., Lakey, P. S. J., Rossich Molina, E., Perraud, V., Wingen, L. M., Xu, J.,  
724 Soulsby, D., Gerber, R. B., Shiraiwa, M. and Finlayson-Pitts, B. J.: Understanding interactions of  
725 organic nitrates with the surface and bulk of organic films: implications for particle growth in the  
726 atmosphere, *Environ. Sci. Processes Impacts*, 20, 1593-1610, 10.1039/C8EM00348C, 2018.
- 727 Virtanen, A., Joutsensaari, J., Koop, T., Kannosto, J., Yli-Pirilä, P., Leskinen, J., Mäkelä, J. M.,  
728 Holopainen, J. K., Pöschl, U. and Kulmala, M.: An amorphous solid state of biogenic secondary  
729 organic aerosol particles, *Nature*, 467, 824-827, 2010.
- 730 Von Domaros, M., Lakey, P. S. J., Shiraiwa, M. and Tobias, D. J.: Multiscale Modeling of Human  
731 Skin Oil-Induced Indoor Air Chemistry: Combining Kinetic Models and Molecular Dynamics, *J.*  
732 *Phys. Chem. B*, 124, 3836-3843, 10.1021/acs.jpcc.0c02818, 2020.



- 733 Worsnop, D. R., Morris, J. W., Shi, Q., Davidovits, P. and Kolb, C. E.: A chemical kinetic model  
734 for reactive transformations of aerosol particles, *Geophys. Res. Lett.*, 29, 57,  
735 10.1029/2002gl015542, 2002.
- 736 Ye, Q., Robinson, E. S., Ding, X., Ye, P., Sullivan, R. C. and Donahue, N. M.: Mixing of secondary  
737 organic aerosols versus relative humidity, *Proc. Natl. Acad. Sci. U.S.A.*, 113, 12649-12654, 2016.
- 738 Ye, Q., Upshur, M. A., Robinson, E. S., Geiger, F. M., Sullivan, R. C., Thomson, R. J. and  
739 Donahue, N. M.: Following Particle-Particle Mixing in Atmospheric Secondary Organic Aerosols  
740 by Using Isotopically Labeled Terpenes, *Chem*, 4, 318-333, 10.1016/j.chempr.2017.12.008, 2018.
- 741 Yli-Juuti, T., Pajunoja, A., Tikkanen, O.-P., Buchholz, A., Faiola, C., Väisänen, O., Hao, L., Kari,  
742 E., Peräkylä, O., Garmash, O., Shiraiwa, M., Ehn, M., Lehtinen, K. and Virtanen, A.: Factors  
743 controlling the evaporation of secondary organic aerosol from  $\alpha$ -pinene ozonolysis, *Geophys. Res.*  
744 *Lett.*, 44, 2562-2570, 10.1002/2016GL072364, 2017.
- 745 You, Y., Smith, M. L., Song, M., Martin, S. T. and Bertram, A. K.: Liquid-liquid phase separation  
746 in atmospherically relevant particles consisting of organic species and inorganic salts, *Int. Rev.*  
747 *Phys. Chem.*, 33, 43-77, 10.1080/0144235x.2014.890786, 2014.
- 748 Zaveri, R. A., Easter, R. C., Shilling, J. E. and Seinfeld, J. H.: Modeling kinetic partitioning of  
749 secondary organic aerosol and size distribution dynamics: representing effects of volatility, phase  
750 state, and particle-phase reaction, *Atmos. Chem. Phys.*, 14, 5153-5181, 10.5194/acp-14-5153-  
751 2014, 2014.
- 752 Zaveri, R. A., Shilling, J. E., Zelenyuk, A., Liu, J., Bell, D. M., D'Ambro, E. L., Gaston, C. J.,  
753 Thornton, J. A., Laskin, A., Lin, P., Wilson, J., Easter, R. C., Wang, J., Bertram, A. K., Martin, S.  
754 T., Seinfeld, J. H. and Worsnop, D. R.: Growth Kinetics and Size Distribution Dynamics of  
755 Viscous Secondary Organic Aerosol, *Environ. Sci. Technol.*, 52, 1191-1199,  
756 10.1021/acs.est.7b04623, 2018.
- 757 Zaveri, R. A., Shilling, J. E., Zelenyuk, A., Zawadowicz, M. A., Suski, K., China, S., Bell, D. M.,  
758 Veghte, D. and Laskin, A.: Particle-Phase Diffusion Modulates Partitioning of Semivolatile  
759 Organic Compounds to Aged Secondary Organic Aerosol, *Environ. Sci. Technol.*, 54, 2595-2605,  
760 10.1021/acs.est.9b05514, 2020.
- 761 Zhang, Y., Chen, Y., Lambe, A. T., Olson, N. E., Lei, Z., Craig, R. L., Zhang, Z., Gold, A., Onasch,  
762 T. B., Jayne, J. T., Worsnop, D. R., Gaston, C. J., Thornton, J. A., Vizuete, W., Ault, A. P. and  
763 Surratt, J. D.: Effect of the Aerosol-Phase State on Secondary Organic Aerosol Formation from  
764 the Reactive Uptake of Isoprene-Derived Epoxydiols (IEPOX), *Environ. Sci. Technol. Lett.*,  
765 10.1021/acs.estlett.8b00044, 2018.
- 766 Zhou, S., Shiraiwa, M., McWhinney, R., Pöschl, U. and Abbatt, J. P. D.: Kinetic limitations in  
767 gas-particle reactions arising from slow diffusion in secondary organic aerosol, *Faraday Discuss.*,  
768 165, 391-406, 10.1039/C3FD00030C, 2013.
- 769 Zhou, S., Hwang, B. C. H., Lakey, P. S. J., Zuend, A., Abbatt, J. P. D. and Shiraiwa, M.:  
770 Multiphase reactivity of polycyclic aromatic hydrocarbons is driven by phase separation and



- 771 diffusion limitations, Proc. Natl. Acad. Sci. U.S.A., 116, 11658-11663, 10.1073/pnas.1902517116,  
772 2019.
- 773 Ziemann, P. J. and Atkinson, R.: Kinetics, products, and mechanisms of secondary organic aerosol  
774 formation, Chem. Soc. Rev., 41, 6582-6605, 2012.
- 775 Zuend, A. and Seinfeld, J. H.: Modeling the gas-particle partitioning of secondary organic aerosol:  
776 the importance of liquid-liquid phase separation, Atmos. Chem. Phys., 12, 3857-3882,  
777 10.5194/acp-12-3857-2012, 2012.  
778  
779